Supplementary Information 2: Detection, analysis and removal of glitches from InSight's seismic data from Mars

1 Theoretical considerations for apparent glitch polarizations

The glitch polarization describes the direction (azimuth and inclination) in which the SEIS sensor assembly (Seismic Experiment for Internal Structure, Lognonné et al., 2019) must be accelerated in order to produce the observed glitch signal on the three sensors U, V and W of the very broadband (VBB) and short-period (SP) seismometer, respectively. Thus, irrespective of analyzing a one-component or a multi-component glitch, we map the non-orthogonal UVW-components (Fig. 1a,c in main paper) into the orthogonal ZNE-components before computing azimuth and inclination of the glitch polarization. For a one-component glitch the non-orthogonality of the VBB components leads to the non-intuitive result in that the glitch azimuth differs slightly from the azimuth of the sensitive direction of the affected sensor while the incidence angle of the same one-component glitch differs by $\sim 12^\circ$ from the sensor's dip angle. We demonstrate this relation in the following.

Projecting the seismometer components from the orthogonal basis vectors Z (positive up), N (positive North), and E (positive East) onto the arbitrarily oriented basis of UVW, we must start with the following linear system of equations:

$$\begin{pmatrix} U \\ V \\ W \end{pmatrix} = \underbrace{\begin{pmatrix} -\sin(\delta_U) & \cos(\delta_U)\cos(\phi_U) & \cos(\delta_U)\sin(\phi_U) \\ -\sin(\delta_V) & \cos(\delta_V)\cos(\phi_V) & \cos(\delta_V)\sin(\phi_V) \\ -\sin(\delta_W) & \cos(\delta_W)\cos(\phi_W) & \cos(\delta_W)\sin(\phi_W) \end{pmatrix}}_{A} \cdot \begin{pmatrix} Z \\ N \\ E \end{pmatrix}, \tag{1}$$

where A represents the base transformation matrix, δ_i the sensor dip of sensor i, and ϕ_i the sensor azimuth of sensor i clockwise from N. Note that sensor dips are defined as positive downwards from the horizontal plane (e.g. Ahern et al., 2012), which is taken into account in A. To reconstruct data recorded in the UVW-system into the ZNE-system, we must use the inverse operation:

$$\begin{pmatrix} Z \\ N \\ E \end{pmatrix} = A^{-1} \cdot \begin{pmatrix} U \\ V \\ W \end{pmatrix}, \tag{2}$$

with A^{-1} the inverse matrix of A. If we now consider a glitch that occurred only on VBB U with an amplitude $U = 1$ ($V = 0, W = 0$), insert those values into Equation 2, and use the following equations to determine the apparent glitch azimuth defined clock-wise from N, AZ, and apparent glitch incidence INC defined as the angle with respect to the Z-axis, it follows:

$$\begin{aligned} AZ &= \text{atan2}\ (E, N) = \text{atan2}\ (A^{-1}_{31}, A^{-1}_{21}) \\ INC &= \text{acos}\left(\frac{\langle [Z,0,0]^T, [Z,N,E]^T \rangle}{\| [Z,0,0]^T \| \cdot \| [Z,N,E]^T \|}\right) = \text{acos}\left(\frac{A^{-1}_{11}}{\sqrt{\left(A^{-1}_{11}\right)^2 + \left(A^{-1}_{21}\right)^2 + \left(A^{-1}_{31}\right)^2}}\right). \end{aligned} \tag{3}$$

We can calculate the inverse matrix elements $(A^{-1})_{j1}$ with the known VBB sensor azimuths $\phi_U = 135.1^\circ$, $\phi_V = 15.0^\circ$ and $\phi_W = 255.0^\circ$, and VBB sensor dips $\delta_U = -29.7^\circ$, $\delta_V = -29.2^\circ$ and $\delta_U = -29.4^\circ$. One finds:

Corresponding author: John-Robert Scholz, scholz@mps.mpg.de

$$\begin{aligned} AZ &= 134.6^\circ \neq 135.1^\circ = \phi_U \\ INC &= 48.5^\circ \neq 60.3^\circ = 90.0^\circ + \delta_U. \end{aligned} \tag{4}$$

Thus, the apparent azimuth and incidence angles of a one-component VBB glitch will *not* point in the direction of the sensitive direction of the affected VBB sensor. Instead, the polarization vector is parallel to the vector cross-product of the remaining two components that do not show the glitch. Due to the similar arrangement of all VBB's sensors (see Fig. 1a in the main paper), the case demonstrated for VBB U holds true for VBB V and VBB W, too. Therefore for all VBB components, a one-component glitch polarization analysis will deliver azimuth angles (almost) parallel to the sensor azimuths and hence be intuitive, whilst incidence angles will be $INC \sim 48^\circ$ (or 132°) as opposed to the sensor incidences of $90.0^\circ + \delta_i \approx 60^\circ$ (or 120°). For multi-component VBB glitches similar considerations disclose the calculated azimuths will also be intuitive, however, for a two-component glitch the incidence must be $INC \simeq 30.0^\circ$–150° (within a plane orthogonal to the third component), whilst for a three-component glitch the incidence can cover the whole parameter space of $INC = 0^\circ$–180°. It follows immediately that any VBB glitch for which we observe an $INC < 30^\circ$ or $INC > 150^\circ$ must, necessarily, involve all three VBB components.

Doing the same exercise for SP, with azimuths of $\phi_U = 285.0^\circ$, $\phi_V = 105.2^\circ$ and $\phi_W = 345.3^\circ$, and dips of $\delta_U = -89.9^\circ$, $\delta_V = 0.0^\circ$ and $\delta_U = 0.0^\circ$ (Fig. 1c in main paper), one finds that for SP U (Z) the azimuth and incidence angles will follow one's intuition closely and be 0° and 0°, respectively. For the horizontal components SP V and SP W the case is different: a SP V glitch will reveal an incidence angle of $INC = 89.9^\circ$–90.1° as expected, but an azimuth of $AZ \sim 075^\circ/255^\circ$, which is not intuitive given its sensor azimuth of $\phi_V = 105.2^\circ$. Similarly for SP W, the incidence angle will be $INC = 89.9^\circ$–90.1° but the azimuth $AZ \sim 015^\circ/195^\circ$, as opposed to the sensor azimuth of $\phi_V = 345.2^\circ$. A direct consequence is that any SP glitch pointing parallel to the SP V or SP W sensor azimuths must be in fact a multi-component SP glitch. For multi-component SP glitches, we did not detect any glitches that occur on the vertical SP U component in combination with either one or two of the horizontal components SP V and SP W. That is, the only multi-component SP glitches are two-component glitches on SP V and SP W. Multi-component SP glitches are therefore always oriented in the horizontal plane.

The message from these theoretical considerations is that our glitch polarization analysis will deliver azimuths and incidence angles that correctly account for the non-orthogonality of VBB and SP; the vectors defined by these angles point into the only physically possible directions for a given one-, two- or three-component glitch, assuming a rigid motion of SEIS. On the other hand, for the interpretations of these angles, it must be born in mind that VBB incidence angles may carry counter-intuitive information whilst SP azimuth angles for one-component glitches will not align with the respective sensor azimuths but diverge by $\sim 30^\circ$.

At this stage we also note that whilst the poles and zeros of the VBB and SP seismometer responses are well determined, the same does not apply fully for the generator constants (gains). In the worst case they may differ up to 10% from the absolute values known by pre-mission tests. To convince ourselves of the correctness of determined glitch azimuths and incidences with respect to these constants we conducted a test: we took the raw data of one- and multi-component glitches of different amplitudes and divided the respective components by their gains that we allowed to vary each by up to $\pm 10\%$. For each permutation, we then rotated into the ZNE-system and performed the polarization analysis. For VBB, we find that glitch azimuths and incidences generally stay within $\pm 5^\circ$ and $\pm 4^\circ$, respectively. For SP, we find that glitch azimuths and incidences generally stay within $\pm 3^\circ$ and $\pm 1^\circ$, respectively, the latter of which is because SP multi-component glitches occur only on the horizontal components. All these values are smaller than the typical errors of polarization measurements and we can therefore assume the resulting glitch patterns to be reliable.

2 Mathematical description of the glitch plus spike origins

Let us consider a general geometry such as depicted in Figure 9 in the main paper where a cross section through a VBB sensor perpendicular to its hinge is graphed. In this figure, the SEIS sensor assembly is rotated around the tip of leg A by a small angle α such that the tip of leg B is raised by $d{\cdot}\alpha$, with d being the distance between the tips of the legs. The sensitive axis of the VBB accelerometer, denoted with the unit vector $\hat{\sigma}$, is inclined relative to the horizontal by the angle δ which is close to -29°, depending on the VBB sensor.

The force of gravity acting on the proof mass M and which the suspension spring has to counterbalance is:

$$F_o = g \cdot M \cdot \sin(\delta), \tag{5}$$

where $g = 3.71\mathrm{m/s}^2$ is the surface gravity on Mars. After the tilting of SEIS by the angle α, the projection of $\vec{g}$ onto the sensitive axes changes and it follows:

$$F = g \cdot M \cdot \sin(\delta + \alpha). \tag{6}$$

The change in acceleration $\ddot{u}$ produced by the tilting thus is:

$$\frac{F - F_o}{M} = \ddot{u} = g \cdot \alpha \cdot \cos(\delta). \tag{7}$$

Since the rotation axis does not go through the center of gravity P of the proof mass M, the rotation leads also to a displacement of the proof mass. In our case this displacement, y, is a small arc segment of a circle with radius $r = \overline{AP}$ around the tip of leg A: $y = r \cdot \alpha$. The accelerometer only senses the projection of this displacement onto its sensitive direction. If we define the unit vector $\hat{r}$ as:

$$\hat{r} = \frac{\vec{AP}}{|\overline{AP}|}, \tag{8}$$

the sensed displacement then becomes:

$$u = r \cdot \alpha \cdot |\hat{r} \times \hat{\sigma}|. \tag{9}$$

What is the time history of this tilt and the simultaneous displacement? As we shall see, the data can be very well modeled by assuming that the time dependence follows a Heavyside function, that is the tilt and the displacements occur over a time interval much shorter than can be resolved with the given sampling interval. In the analyzed glitches we see little to no indication for a slowly progressing tilt.

Now we have to account for the fact that inertial accelerometers like the VBB and SP seismometers in the SEIS package have a frequency dependent sensitivity to ground motion. This is described by the impulse response $T(t)$. In the time domain the output of the seismometer then becomes the convolution of the input convolved with the impulse response where the input can be the ground displacement, ground velocity or ground acceleration. The seismometer response to a Dirac impulse in displacement, velocity or acceleration are denoted $T_{DIS}(t)$, $T_{VEL}(t)$ and $T_{ACC}(t)$, respectively. They are related by:

$$T_{DIS}(t) = \dot{T}_{VEL}(t) = \ddot{T}_{ACC}(t). \tag{10}$$

The summed output U from the acceleration step due to the tilting at time t_o and the associated displacement step then becomes:

$$U(t) = g\alpha\cos(\delta) \cdot H(t - t_o) * T_{ACC}(t) + r \cdot \alpha \cdot |\hat{r} \times \hat{\sigma}| \cdot H(t - t_o) * T_{DIS}(t). \tag{11}$$

Since the impulse responses due to ground displacement is the second time derivative of the impulse response due to ground accelerations, we anticipate that the acceleration step produces a low-frequency response while the displacement step should be dominated by high frequencies. This is exactly what the Figures 1 and 6 in the main paper show. The step in acceleration leads to the glitch while the step in displacement leads to the high-frequency spike.

When modeling the glitches and their spikes, we obtain the time of the occurrence of the glitch, t_o, as well as the amplitude of acceleration and displacement steps. From the acceleration step, $\ddot{u}$, we can infer the tilt angle α based on Equation (7). What is not possible is to infer the location of the rotation axis given the observed step in displacement, u, and the rotation angle α. Only if we assume that $\hat{r}$ and $\hat{\sigma}$ are at right angles can we infer an effective distance $r_{eff} = u/\alpha$ between rotation axis and the proof mass.

To see if the mathematical simplifications are justified we plug in numbers for the glitch in Figure 6 in the main paper (see also Table 2 in main paper): the step in acceleration is 259 nm/s^2. The inferred tilt of SEIS which is responsible for that glitch is then:

$$\alpha = \frac{\ddot{u}}{g \cdot \cos(\delta)} = \frac{259\,\mathrm{nm/s^2}}{3.71\,\mathrm{m/s^2} \cdot \cos(29.3^\circ)} \simeq 80.0\,\mathrm{nrad}. \tag{12}$$

So indeed, these are tiny tilt angles. The displacement obtained from modeling the spike of this glitch is $u = 3\mathrm{nm}$. The effective distance r_{eff} of the rotation axis away from the center of gravity of the proof mass is then:

$$r_{eff} = \frac{u}{\alpha} = \frac{3\,\mathrm{nm}}{80\,\mathrm{nrad}} = 3.7\,\mathrm{cm}. \tag{13}$$

In summary, we have shown that an accelerometer which gets rotated around a horizontal axis that does not go through the center of gravity of the proof mass senses two signals: the response to the tilt and the response to the resulting displacement. While the former shows up in the data as the low frequency glitch, the latter leads to the high-frequency spike signal.

3 Additional Figures

In this section, we provide some additional figures we have created while investigating the glitch plus spike phenomenon. We will not put each figure into context but would simply like to refer to their captions for understanding.

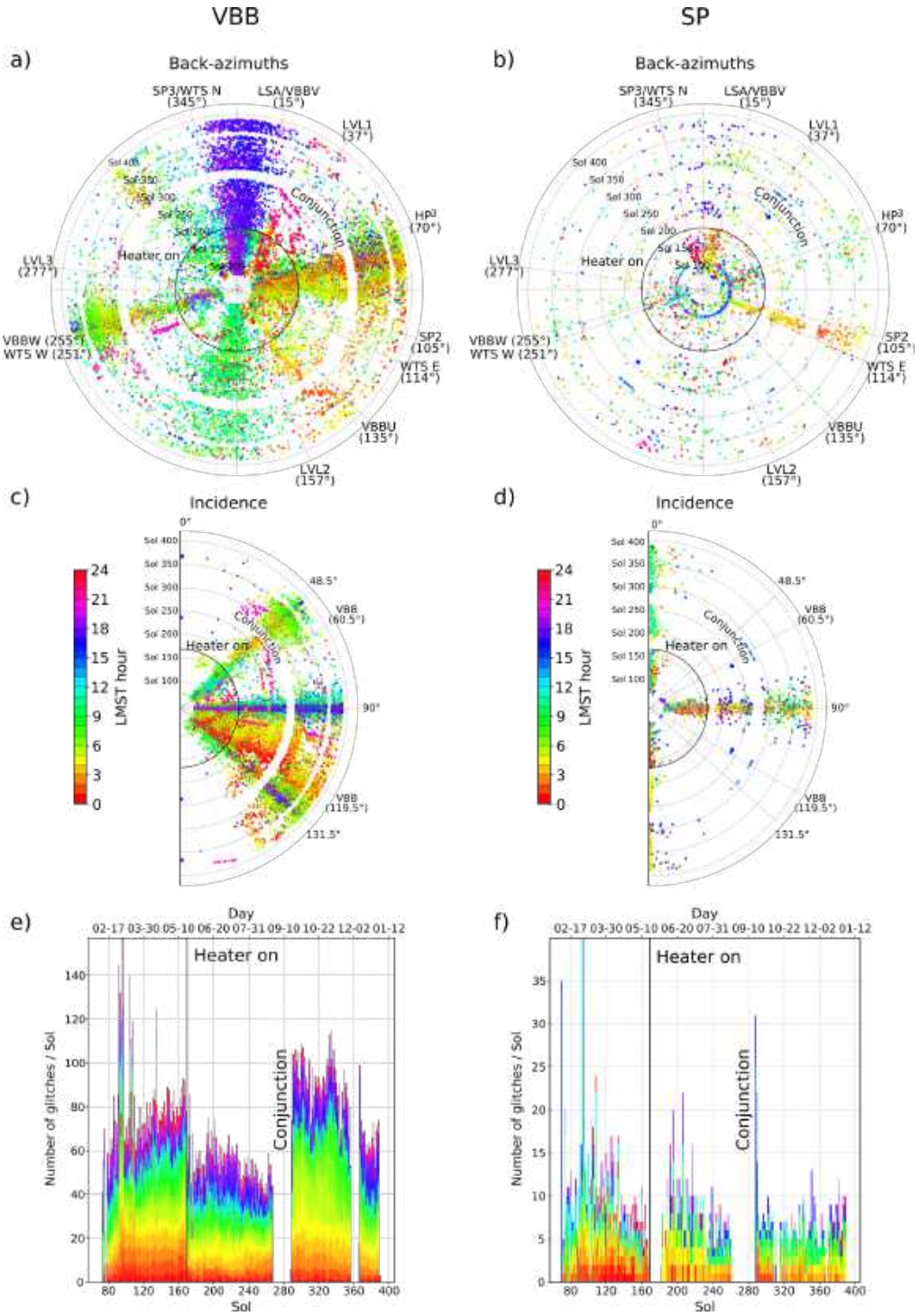

Figure SI2-1: Detected VBB glitches for 2019 (MPS method), corresponding to Figures 2–5 in the main paper. Here, all glitches have been combined into one plot instead of detailing certain aspects in three different plots.

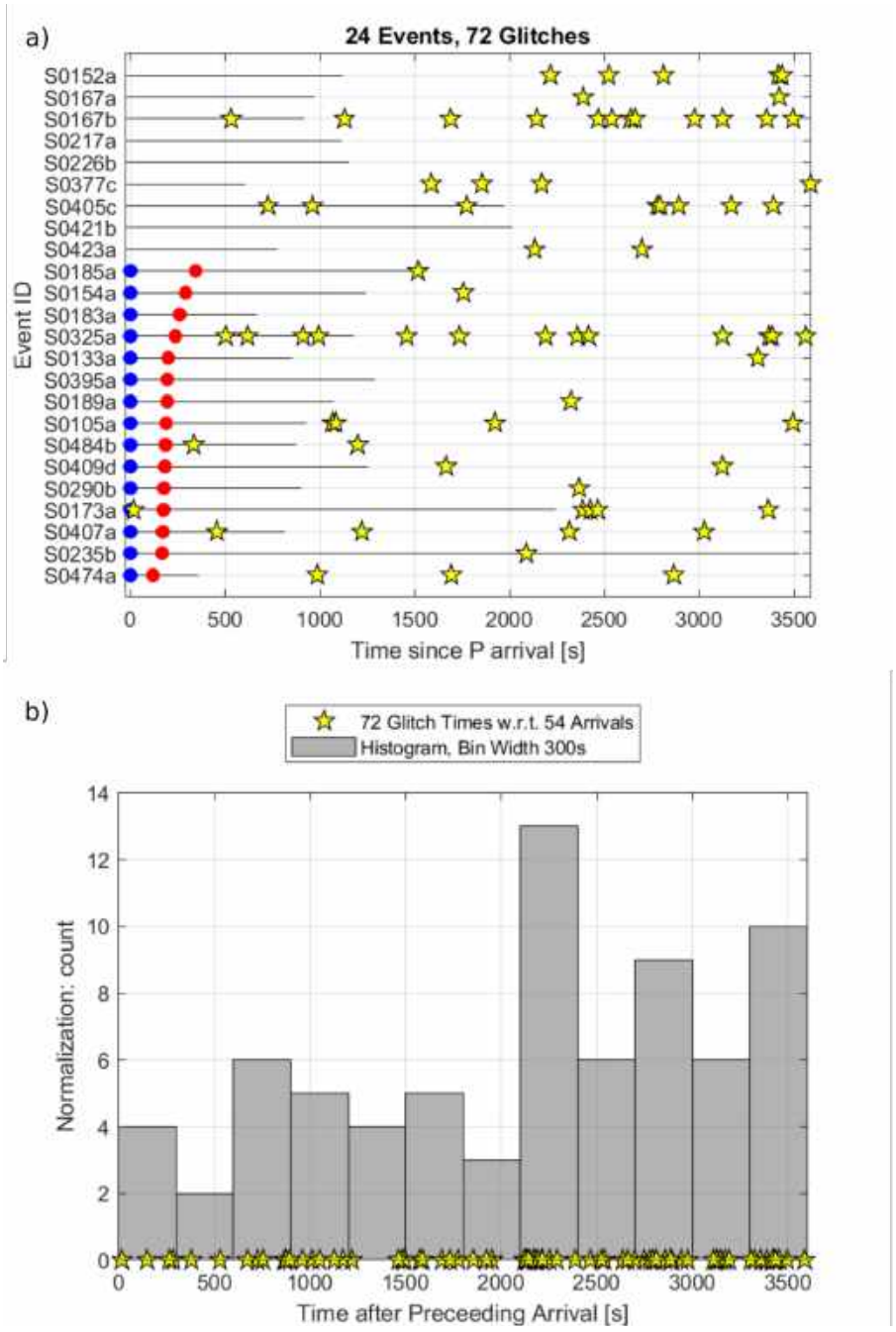

Figure SI2-2: Correlation of detected glitches (MPS method) with marsquake arrivals as identified by the MarsQuakeService (Clinton et al., 2018, for catalogue see: InSight Marsquake Service, 2020). To investigate a possible triggering of glitches by seismic arrivals, we compare detected glitches with low-frequency and broadband events of qualities A–C ('A' is best quality). a) All detected glitches within one hour after the P-arrival, or the beginning of the visible signal where no clear arrival could be identified. Events with arrivals are sorted by S-P time, others by sol. Blue: P arrivals, red: S arrivals, horizontal lines: time windows of visible quake signal, stars: glitches. b) Time between glitch and the last preceding arrival (P or S). Stars: Glitches, Histogram: number of glitches in 5 min time windows. Only 6 of 72 considered glitches occur within 10 min after the last arrival. Given this small number, we do not consider the difference between the first and the second bin as significant, indicating that glitches during seismic events are not occurring significantly more than during periods of no seismic events.

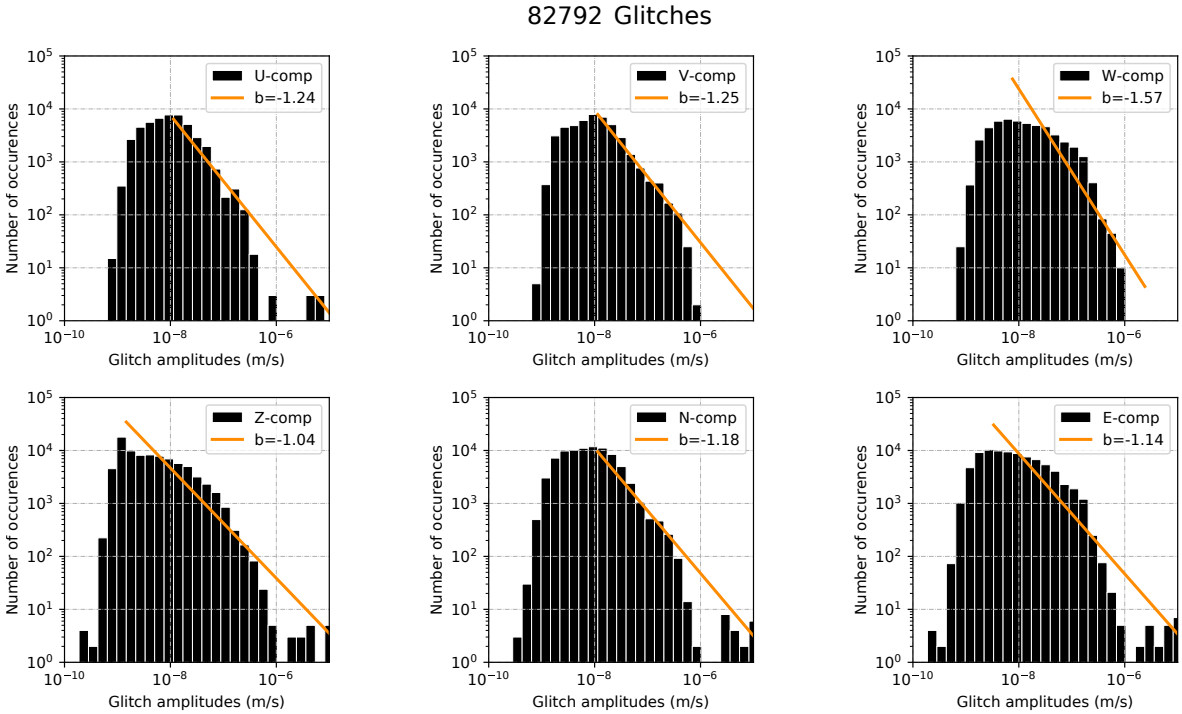

Figure SI2-3: 2019 VBB glitch histograms per component, detected by the MPS method with more sensitive glitch detector settings than utilised in the main paper. We find a seemingly stable Gutenberg-Richter relation with b-values of ∼1–1.3, and roll-off glitch amplitudes of ∼1e-8 m/s (RAW data corrected for gain. The velocity response is flat for periods shorter than 16 seconds). This may indicate an underlying stochastic process behind the glitch production that, perhaps, points once more to thermal causes of glitches.

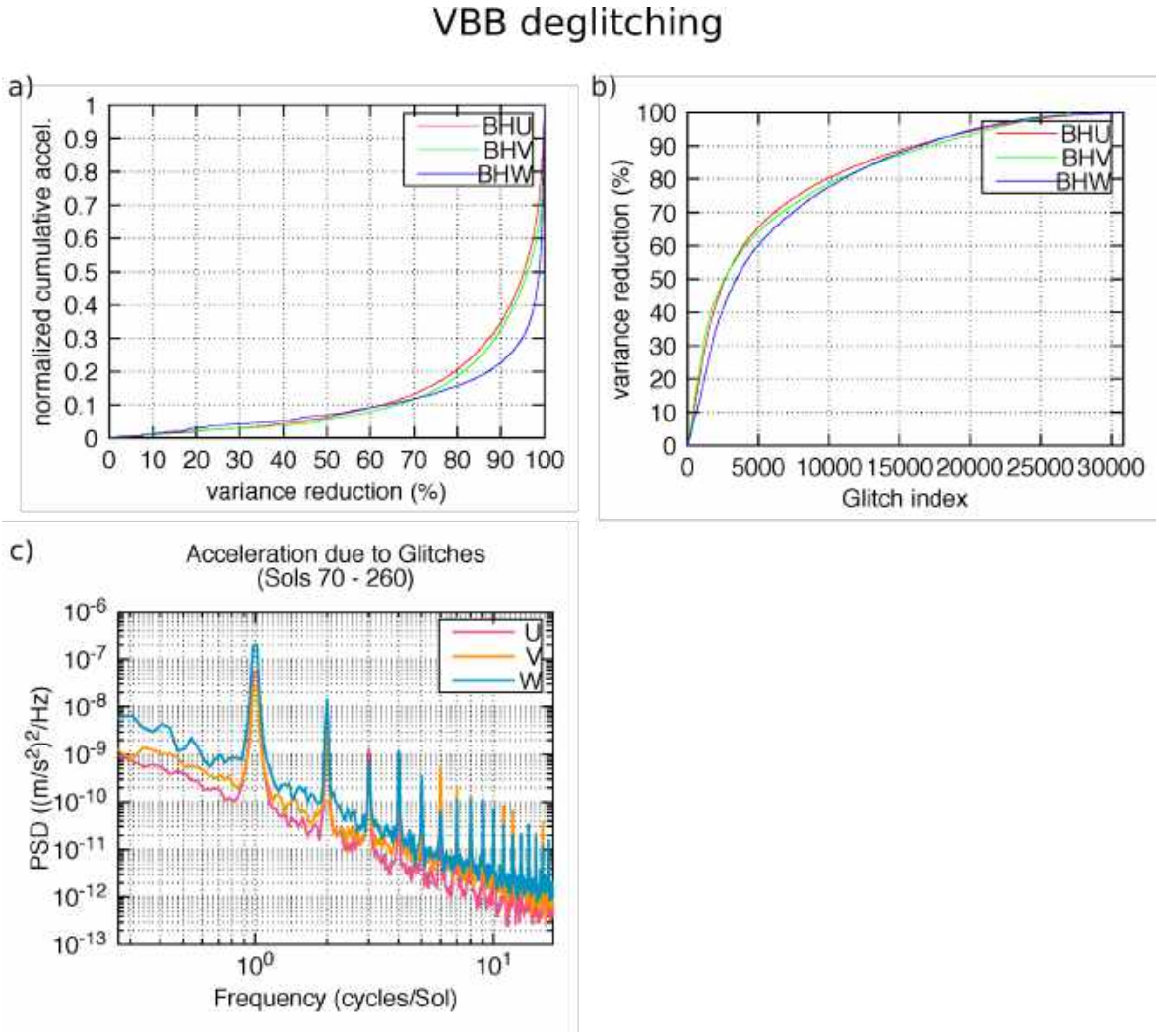

Figure SI2-4: a) Cumulative contribution of glitches to the total acceleration signal. The glitches have been sorted by their variance reduction obtained from the glitch modeling. This panel shows that poorly modeled glitches (variance reduction of less than e.g. 85%) make up only a small fraction of the total acceleration signal: 25%, 25% and 18% for U, V and W respectively. b) Glitches sorted by variance reduction: For the chosen sensitivity of the MPS detector in the main paper and for the time interval Sol 70 through Sol 260, there are 13000 glitches with variance reduction less than 85% and 18000 with variance reduction greater than 85%. Taken together panels (a) and (b) show that the largest contribution in terms of signal amplitude comes from the large and well modeled glitches. In terms of signal power the contribution of the large and well modeled glitches becomes even more dominant. c) Contribution of all modeled glitches to the acceleration background for the three VBB components U, V and W. All glitches for Sols 70 through 260 for which the variance reduction in the glitch modeling stage exceeded 85% are included. A glitch corresponds to a step in acceleration at a particular time. Here we have added up in the time domain 18000 step functions, one for each glitch, with the step size corresponding to the glitch amplitude. The power spectral density of the resulting stair case like, noise free time series has been analyzed. The harmonics at integer multiples of 1 cycle/Sol are a strong indication that the glitches have a thermal cause. This analysis is a complementary method to quantify the contribution of glitches to the VBB analysis presented in figure 10a of the main paper.

References

Ahern, T. K., Buland, R., Halbert, S., Styles, Ray, Skjellerup, Kris, Casey, Rob, ... Trabant, Chab (2012). *SEED Reference Manual.* IRIS.

Clinton, J., Giardini, D., Böse, M., Ceylan, S., van Driel, M., Euchner, F., ... Teanby, N. A. (2018, December). The Marsquake Service: Securing Daily Analysis of SEIS Data and Building the Martian Seismicity Catalogue for InSight. *Space Science Reviews*, *214*(8), 133. doi: 10.1007/s11214-018-0567-5

InSight Marsquake Service. (2020). *Mars seismic catalogue, insight mission; v2 2020-04-01.* ETHZ, IPGP, JPL, ICL, ISAE-Supaero, MPS, Univ. Bristol. Retrieved from `http://www.insight.ethz.ch/seismicity/catalog/v2` doi: 10.12686/a7

Lognonné, P., Banerdt, W. B., Giardini, D., Pike, W. T., Christensen, U., Laudet, P., ... Wookey, J. (2019, January). SEIS: Insight's Seismic Experiment for Internal Structure of Mars. *Space Science Reviews*, *215*(1). doi: 10.1007/s11214-018-0574-6